INSTITUTE OF PHYSICS PUBLISHING MEASUREMENT SCIENCE AND TECHNOLOGY

Meas. Sci. Technol. **18** (2007) 265–274 doi:10.1088/0957-0233/18/1/033

Two-dimensional optical accelerometer based on commercial DVD pick-up head

Chih-Liang Chu[1], **Cha-Hao Lin**[1] **and Kuang-Chao Fan**[2]

[1] Department of Mechanical Engineering, Southern Taiwan University of Technology, Tainan, Taiwan, Republic of China
[2] Department of Mechanical Engineering, National Taiwan University, Taipei, Taiwan, Republic of China

E-mail: cliang@mail.stut.edu.tw

Received 22 August 2006, in final form 16 November 2006
Published 12 December 2006
Online at stacks.iop.org/MST/18/265

Abstract
This study develops a low-cost, highly sensitive two-dimensional optical accelerometer based on a commercially available DVD optical pick-up head. Vibrations of the structure of interest cause a change in the angle of the seismic mass within the accelerometer. The relative movement between the seismic mass and the base produces a change in the distribution of a focused light spot on the surface of a four-quadrant photodetector. The resulting change in the output of the voltage signals by the photodetector is then used to calculate the corresponding acceleration of the base. The experimental results indicate that the resonant frequencies of the accelerometer in the X- and Y-axis directions are 92.75 Hz and 92.87 Hz, respectively. Furthermore, the useful frequency range of the accelerometer is found to be approximately 20% of its resonant frequency. The sensitivities of the accelerometer in the X- and Y-axis directions are 22.9 V/g and 21.3 V/g, respectively. Finally, the noise equivalent acceleration (NEA) of the accelerometer is found to be less than 30 μg Hz$^{-1/2}$ over the frequency range 0.5–50 Hz.

Keywords: accelerometer, optical sensor, DVD pick-up head

(Some figures in this article are in colour only in the electronic version)

1. Introduction

As the technical capabilities of machines designed for use in high-precision industries continue to advance, the need to measure vibration with a higher degree of precision and to develop enhanced vibration isolation schemes is becoming increasingly important. The vibration generated by footsteps in a laboratory is typically of the order of 1–3 Hz, while that of movements of the Earth's crust lies in the range of 0.1–10 Hz. Accordingly, modern vibration isolation schemes for precision mechanical equipment are designed with vibration isolation capabilities of less than 1 Hz. In other words, the accelerometers used in these schemes are designed specifically for low frequency range measurements.

In its simplest form, an accelerometer employs a displacement or angle sensor to record the relative movement between a seismic mass and the base, and then derives the acceleration acting on the base from the displacement signal [1]. The published literature describes many different displacement or angle sensing techniques, including variable capacitance, piezoelectric, piezoresistive, reluctive, magnetic, strain and so forth [2, 3]. However, the use of optical sensing techniques in developing two-dimensional accelerometers has attracted relatively less attention. Fang [4, 5] applied a high refractive index prism and an orthogonal holographic grating to develop a laser-based sensor to measure the two-dimensional angular changes of a moving target. The proposed sensor was capable of measuring two-dimensional angular variations in the range $\pm 35^\circ$ with a measurement resolution of $\pm 0.01^\circ$. Fang applied the laser angle sensor to construct an optical accelerometer for measuring the two-dimensional acceleration of moving objects. The accelerometer demonstrated a measurement range of 5–100g with a measurement error of not more than 0.1g. Dinev *et al* [6, 7] presented a two-dimensional fibre optic accelerometer. In their design, the optical fibre was arranged as a cantilever beam, i.e. fixed

 © 2007 IOP Publishing Ltd Printed in the UK

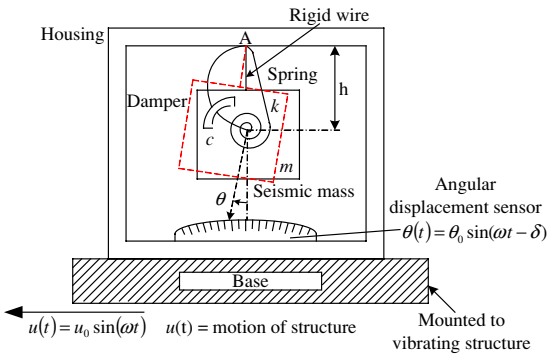

Figure 1. Schematic illustration of a typical optical accelerometer.

at one end and unsupported at the other, and a dual-axis position photosensor was fixed in place facing the free end of this 'cantilever'. Vibrations of the structure of interest produced a deflection of the cantilever tip, causing the focused light spot to move across the surface of the photosensor. The acceleration was then calculated from the corresponding change in the photosensor output signal. The authors showed that the accelerometer could measure the vibrational amplitude and frequency simultaneously in two perpendicular directions with a maximum amplitude measurement range of 400 μm, a resolution of less than 0.5 μm and a linearity error of not more than 0.1%.

The design of accelerometers based on optical principles tends to be more complicated than those based on conventional techniques. Furthermore, optical accelerometers are generally more expensive than other types of accelerometer. Therefore, optical accelerometers find only limited commercial use at present. Nonetheless, such instruments offer considerable potential for high-resolution angle measurements and therefore merit further investigation.

The optical pick-up technology within today's commercially available DVD players is well developed and comparatively inexpensive. The optical and electronic circuitry designs of modern DVD players, and the excellent focusing characteristics of their pick-up heads, are ideally suited to the development of a new generation of low cost optical metrology applications. The published literature presents various applications of the DVD pick-up head, including autocollimators [8], velocimeters [9], profile measurement devices [10, 11], straightness measurement instruments [12], confocal compact scanning systems in optical microscopes [13] and one-dimensional optical accelerometers [14]. The objective of the present study is to exploit the proven technology of a commercially available DVD pick-up head to develop a low-cost, high-precision two-dimensional optical accelerometer.

2. Operational principles

2.1. Basic principle of accelerometer

As implied by its name, an accelerometer measures vibration on the basis of a detected acceleration signal. Figure 1 illustrates the design of a typical optical accelerometer, which as shown, comprises a spring, a damper, a seismic mass and an angular displacement sensor arranged within a housing attached to a base. In operation, the base is mounted on the vibrating structure of interest and the relative displacement between the seismic mass and the base is recorded by the angular displacement sensor. The magnitude of the acceleration acting on the base is then calculated, and the vibration frequency subsequently derived.

Balancing the forces acting on the seismic mass, m, yields

$$I_A\ddot{\theta}(t) + c\left[\dot{\theta}(t) - \frac{\dot{u}(t)}{h}\right] + k\left[\theta(t) - \frac{u(t)}{h}\right] = 0, \qquad (1)$$

where I_A is the mass moment of inertia of the seismic mass, $\theta(t)$ is the absolute angular displacement of the seismic mass, $u(t)$ is the absolute displacement of the structure and t is the time.

In the following derivations, an assumption is made that the base of the accelerometer performs a simple harmonic motion of the form $u(t) = u_0 \sin(\omega t)$, where ω is the frequency of vibration. The relative angular displacement between the seismic mass and the base is given by $\psi(t) = \theta(t) - \frac{u(t)}{h}$. Substituting the expressions for $\psi(t)$ and $u(t)$ into equation (1) yields

$$I_A\ddot{\psi}(t) + c\dot{\psi}(t) + k\psi(t) = \frac{I_A}{h}\omega^2 u_0 \sin(\omega t). \qquad (2)$$

Solving equation (2) for the relative angular displacement, $\psi(t)$, gives

$$\psi(t) = \frac{\omega^2 u_0/h}{\sqrt{\left(\omega_n^2 - \omega^2\right)^2 + (2\xi\omega_n\omega)^2}} \times \sin\left[\omega t + \left(-\tan^{-1}\frac{2\xi\omega_n\omega}{\omega_n^2 - \omega^2}\right)\right], \qquad (3)$$

where $\omega_n = \sqrt{k/I_A}$ and $\xi = c/(2I_A\omega_n)$ are the resonant frequency and the damping ratio of the accelerometer, respectively.

Multiplying both sides of equation (3) by ω_n^2 gives

$$h\omega_n^2\psi(t) = \frac{1}{\sqrt{(1-r^2)^2 + (2\xi r)^2}} u_0\omega^2 \sin(\omega t - \delta), \qquad (4)$$

where r is the frequency ratio, given by $r = \omega/\omega_n$.

The amplitude ratio, $h\psi_0/u_0$, and phase shift, δ, in equation (4) can be expressed, respectively, as

$$\frac{h\psi_0}{u_0} = \frac{r^2}{\sqrt{(1-r^2)^2 + (2\xi r)^2}}; \qquad \delta = \tan^{-1}\frac{2\xi r}{1-r^2}. \qquad (5)$$

Since the acceleration imposed on the base via the vibrating structure is given by $\ddot{u}(t) = -u_0\omega^2\sin(\omega t - \delta)$, when $\omega/\omega_n \ll 1$, the right side of equation (4) becomes $-\ddot{u}(t)$. Therefore, multiplying the value of $\psi(t)$ by $h\omega_n^2$ yields the acceleration acting on the base. Clearly, if the relative angular displacement, $\psi(t)$, between the seismic mass and the base can be measured, the acceleration acting on the base can be obtained. In a novel approach, the present study measures the relative angle between the seismic mass and the base using a two-dimensional angle measurement probe based on the optical pick-up head of a commercial DVD.

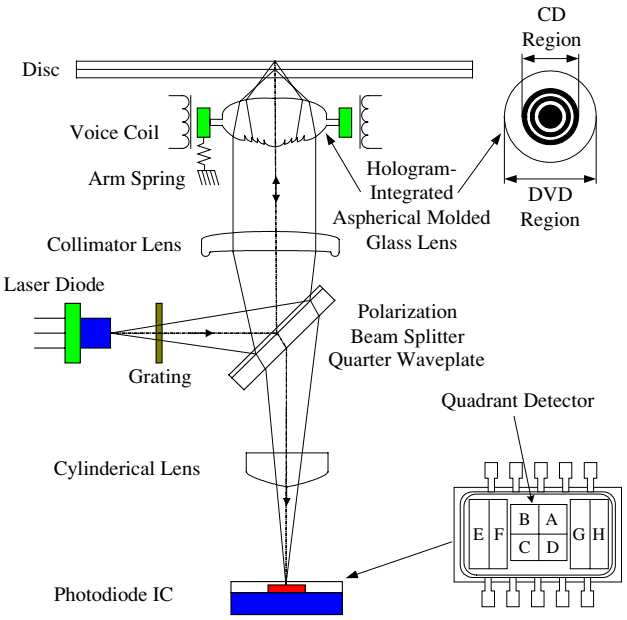

Figure 2. Structure of a commercial DVD/CD pick-up head.

2.2. DVD pick-up head

2.2.1. Principle and modification of DVD pick-up head. Figure 2 illustrates the basic components and operating mechanisms of a commercial DVD pick-up head. Initially, a laser diode generates a beam of light, which passes through a diffraction grating, where it is split into three separate beams. These beams pass through a polarization beam splitter, a quarter wavelength plate, a collimator lens and finally through an objective lens, which focuses the beams upon the surface of the DVD disk. The beams are then reflected back along their original paths until they pass through the polarization beam splitter, at which point they enter a cylindrical lens and are projected onto a four-quadrant photodiode. The photodiode outputs a focus error signal (FES) whose magnitude is dependent upon the distribution of the main beam spot across its four quadrants. After an appropriate processing of the FES, the resulting signal is used to drive the voice coil motor (VCM) in such a way that the objective lens is shifted to a position at which its focal point is returned to the surface of the disk. The displacement of the VCM is then used to determine the surface profile variation of the disk.

Figure 3 presents a schematic illustration of the two-dimensional angle sensor developed in this study. As shown, the DVD pick-up head (Sony KHM-210AAA, 650 nm wavelength [15]) is modified by removing the diffraction grating, the objective lens and the VCM, and then adding a plane mirror. The original four-quadrant photodiode is retained as a light intensity detector. The stability of the laser output power is ensured by using a specially designed power supply integrated with an automatic power control (APC) feedback circuit (not shown).

In the two-dimensional angle measurement system developed in this study, the laser beam is projected onto the plane mirror, and the reflected laser beam is then focused at the centre of the four-quadrant photodiode. When the angle of the plane mirror changes, the position of the focused

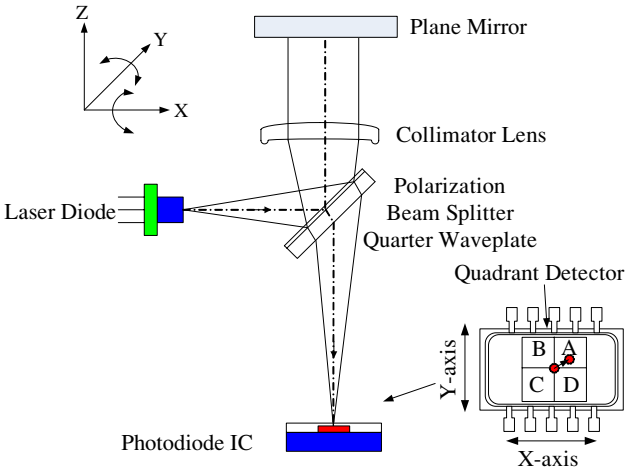

Figure 3. Two-dimensional angle measurement system.

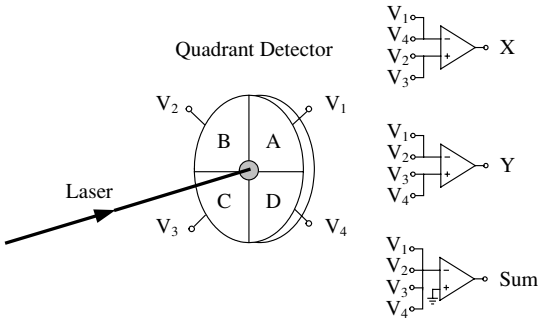

Figure 4. Relationship between focused light spot position on four-quadrant photodetector and corresponding output voltages.

light spot shifts across the surface of the photodiode. As shown in figure 4, the photodetector transforms the incident energy of the focused light spot into electrical current signals. Deviations of the focused light spot from the centre of the photodiode produce corresponding changes in the magnitudes of the electrical signals output by the four quadrants. By applying an appropriate resistance to the electrical current signals, corresponding voltage signals are obtained, and changes in the magnitudes of these voltages can then be used to determine the incident position of the focused light spot on the photodiode. In the current four-quadrant photodetector, the X- and Y-coordinates of the focused light spot are related to the voltage signals of the individual quadrants by the following expressions:

$$X = K\frac{(V_1 + V_4) - (V_2 + V_3)}{V_s} \tag{6}$$

$$Y = K\frac{(V_1 + V_2) - (V_3 + V_4)}{V_s}, \tag{7}$$

where V_i is the voltage of quadrant i, where $i = 1, \ldots, 4$, K is a constant, and V_s is the sum of the four quadrant voltages, i.e. $V_s = V_1 + V_2 + V_3 + V_4$.

2.2.2. Laser beam intensity distribution. If the laser chamber is in the lateral electromagnetic resonate (TEM_{00}) mode, the intensity of the generated beam has a Gaussian distribution

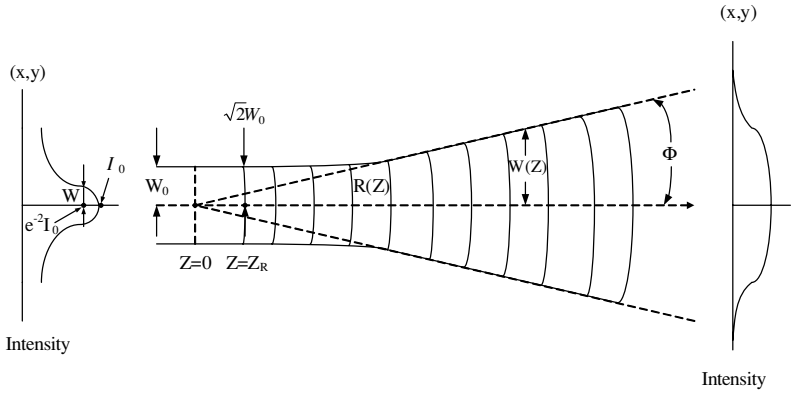

Figure 5. Gaussian laser beam intensity distribution.

and the beam is therefore referred to as a Gaussian beam. As shown in figure 5, the electrical field of this Gaussian beam can be expressed as

$$E(r,z) = \underbrace{E_0 \frac{W_0}{W(z)} \times \exp\left(-\frac{r^2}{W^2(z)}\right)}_{A} \times \underbrace{\exp\left\{-\mathrm{j}\left[kz - \tan\left(\frac{z}{z_R}\right)\right]\right\}}_{B} \times \underbrace{\exp\left[-\mathrm{j}k\frac{r^2}{2R(z)}\right]}_{C}. \tag{8}$$

In equation (8), term A is the amplitude factor and is a function of $r = (x^2 + y^2)^{1/2}$, term B describes the phase change of the light wave along the longitudinal (z) direction and term C describes the phase change of the light wave along the radial (r) direction. Furthermore, W_0 is the beam waist radius when the wave front curvature radius $R(0) \to \infty$ and the wave front curvature becomes a plane. Finally, $W(z)$ and $R(z)$ are the radii of the spot size and the wave front curvature at a distance z from the waist, respectively. When $k = 2\pi/\lambda$ and the origin ($z = 0$) is located at the waist, then

$$W(z) = W_0\left[1 + \left(\frac{\lambda z}{\pi W_0^2}\right)^2\right]^{1/2} = W_0\left[1 + \left(\frac{z}{z_R}\right)^2\right]^{1/2} \tag{9}$$

$$R(z) = z\left[1 + \left(\frac{\pi W_0^2}{\lambda z}\right)^2\right] = z\left[1 + \left(\frac{z_R}{z}\right)^2\right] \tag{10}$$

where $z_R = \pi W_0^2/\lambda$ is defined as the Rayleigh range and is located at a plane positioned at a standoff distance $z = z_R$ from the waist such that the cross-sectional area of the beam spot is exactly twice that of the waist area [$W(z_R) = \sqrt{2}W_0$] and the radius of the wave front curvature, R, is at its minimum.

When the beam propagating distance $z \gg z_R$, $R \approx z$ and $W \approx \lambda z/\pi W_0$, the Gaussian beam appears as a light emitted from a point at the waist. Under these conditions, the divergence angle of the beam has the form

$$\phi = \frac{\mathrm{d}W(z)}{\mathrm{d}z} = \frac{W_0}{z_R} = \frac{\lambda}{\pi W_0}. \tag{11}$$

The Gaussian beam characteristics are determined by W_0 and λ. Since the electric field of the light wave changes very quickly, metrology applications are generally based on the intensity of the light wave. The light intensity distribution is given by the product of equation (8) and its complex conjugate, and can be expressed in Cartesian coordinates as follows:

$$I = E \cdot E^* = I_0 \exp\left\{\frac{-2[(x - x_0)^2 + (y - y_0)^2]}{W^2}\right\}, \tag{12}$$

where x_0 and y_0 are the coordinates of the beam centre, $I_0 = I_{\max}$ is the light intensity at the beam centre and W is the cross-sectional radius of the Gaussian beam.

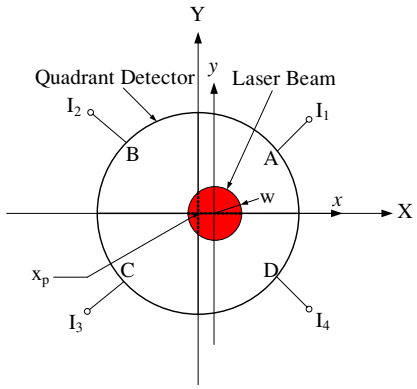

Figure 6. Schematic diagram of laser beam scanning across four-quadrant photodetector along the X-axis.

2.2.3. Mathematical model of laser beam scanning of four-quadrant photodetector. As shown in figure 6, the origin of the X- and Y-axis coordinate system is fixed at the centre of the four-quadrant photodetector, while the origin of the x- and y-axis coordinate system is fixed at the centre of the light spot and moves with the light spot as it scans across the photodetector. When the laser beam scans across the four-quadrant photodetector in the X-axis direction, the relationship between the X-coordinate of the light spot and the intensity signals of the individual quadrants is given by

$$S(x_p) = [(I_1 + I_4) - (I_2 + I_3)]_{x=x_p}$$
$$= \int_{-\infty}^{\infty}\int_{x_p}^{\infty} I(x,y)\,\mathrm{d}x\,\mathrm{d}y - \int_{-\infty}^{\infty}\int_{-\infty}^{x_p} I(x,y)\,\mathrm{d}x\,\mathrm{d}y$$

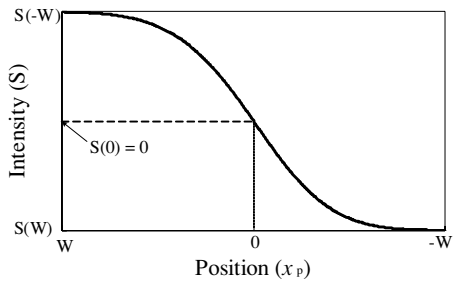

Figure 7. Variation of light signal intensity as scanning position shifts from $-W$ to W.

$$= \int_{-\infty}^{\infty}\int_{x_p}^{\infty} I_0 \exp\left\{\frac{-2[(x-x_0)^2+(y-y_0)^2]}{W^2}\right\} \mathrm{d}x\,\mathrm{d}y - \int_{-\infty}^{\infty}\int_{-\infty}^{x_p} I_0 \exp\left\{\frac{-2[(x-x_0)^2+(y-y_0)^2]}{W^2}\right\} \mathrm{d}x\,\mathrm{d}y,$$

$$= I_0\left(\frac{\pi W^2}{2}\right)^{\frac{1}{2}}\left\{\int_{x_p}^{\infty} \exp\left[\frac{-2(x-x_0)^2}{W^2}\right]\mathrm{d}x - \int_{-\infty}^{x_p} \exp\left[\frac{-2(x-x_0)^2}{W^2}\right]\mathrm{d}x\right\} \quad (13)$$

where x_p denotes the position of the centre of the four-quadrant photodetector on the x-axis and I_i is the light intensity of quadrant i, where $i = 1, \ldots, 4$.

From equation (13), it can be seen that x_p lies in the range $-W$ to W. Figure 7 plots the variation of the light intensity signal with the X-coordinate position of the scanning spot.

The signal shown in figure 7 can be normalized by dividing the light intensity signal value at a particular X-coordinate of the light spot by the total laser intensity signal, i.e.

$$\bar{S}(x_p) = \frac{S(x_p)}{I_s} = \frac{S(x_p)}{\int_{-\infty}^{\infty}\int_{-\infty}^{\infty} I(x,y)\,\mathrm{d}x\,\mathrm{d}y} = \frac{2}{I_0\pi W^2}S(x_p), \quad (14)$$

where I_s is the sum of the individual light intensities of the four quadrants, i.e. $I_s = I_1 + I_2 + I_3 + I_4$.

3. Design, analysis and fabrication of two-dimensional accelerometer

Equation (4) shows that increasing the resonant frequency of the accelerometer, e.g. by increasing the elastic stiffness, k, or decreasing the seismic mass, m, increases the useful frequency range. However, for a constant acceleration acting on the base, increasing the elastic stiffness or decreasing the seismic mass leads to a reduction in the amplitude of the seismic mass, ψ_0. Therefore, the output signal of the angular displacement sensor is reduced and the accuracy of the angular displacement measurement is correspondingly diminished.

Generally, the useful frequency range and error bound of an accelerometer depend on the particular application for which it is intended. In the present study, the accelerometer

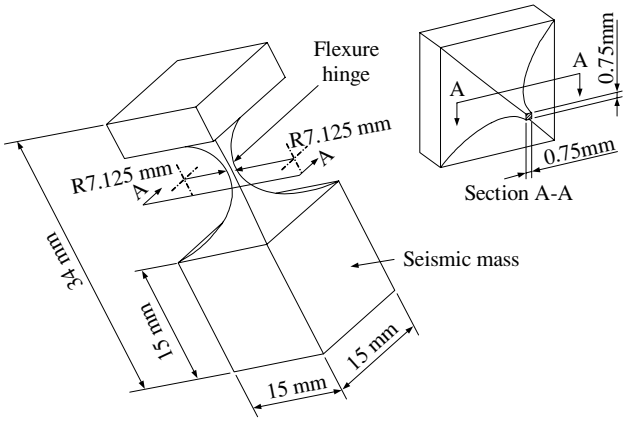

Figure 8. Schematic of notch-type flexure hinge.

is designed to measure the movement of the Earth's crust. Therefore, a nominal frequency of 10 Hz is specified as the useful frequency range. The accuracy of the angular displacement measurement is adversely affected if the resonant frequency is too high. Accordingly, the resonant frequency of the current accelerometer is assigned a nominal design value of 100 Hz. Assuming that the structure of the accelerometer is fabricated from a low damping ratio material, specifying the useful frequency range of the optical accelerometer as 10% of the resonant frequency ensures that the calculated acceleration results are accurate to within approximately 1%.

Since the objective in this study is to develop a two-dimensional optical accelerometer, the seismic mass must be capable of performing two-dimensional motion. Accordingly, the accelerometer is based on the notch-type flexure hinge shown in figure 8, where the hinge acts as the accelerometer spring and the structure below the hinge acts as the seismic mass. Flexure hinges have many advantages, including no friction losses, no lubrication requirements, no hysteresis, a compact size, a straightforward manufacturing process and no maintenance requirements. As shown, the two-axis flexure hinge is designed with symmetrical notches of equal length and equal radius. This design limits the seismic mass to movements only in the X- and Y-axis directions and ensures that the two axes have the same frequency response. Flexure hinges are characterized by relatively low rotation levels, and therefore movements of the seismic mass enable highly precise measurements of changes in the angular displacement to be obtained. However, flexure hinges suffer a major drawback in that their rotation is not pure because the hinge is sensitive not only to axial loading, shearing and torsion, but also to bending. Unlike classical rotation joints in which the centre of rotation remains in a fixed position, the 'rotation centre' of a flexure hinge (generally assumed to be its midpoint) is not fixed during the relative rotation produced by the flexure, but is displaced under the action of the combined load. This characteristic of flexure hinges has a direct impact on the performance of the current accelerometer since it results in cross-talk between the X- and Y-axes during operation. Analysing the effect and extent of cross-talk in the accelerometer using theoretical methods is complex, and hence this study quantifies the cross-talk effect directly using an experimental method.

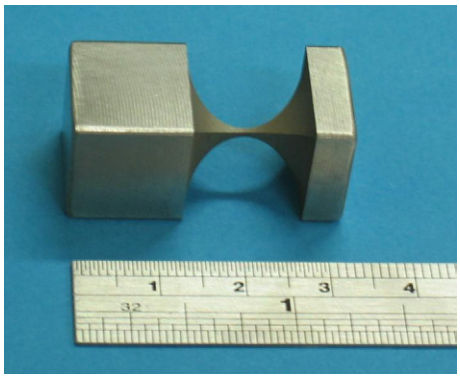

Figure 9. Photograph of notch-type flexure hinge.

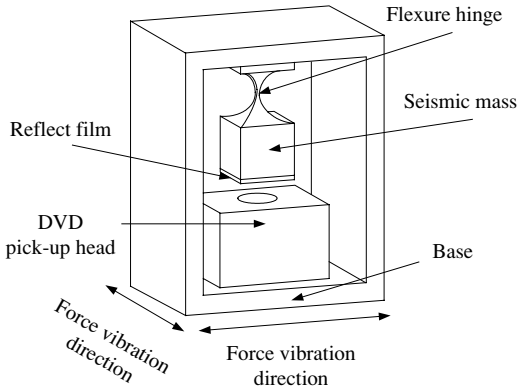

Figure 10. Schematic illustration of two-dimensional optical accelerometer.

Figure 9 presents a photograph of the current flexure hinge. The combined flexure and seismic mass structure was machined from a single block of S304 stainless steel using an electro-discharge machining (EDM) technique with machining tolerances of ± 5 μm specified throughout.

A three-dimensional geometric model of the seismic structure was constructed using ANSYS FEM software with 45 8-node solid hexahedron elements. In constructing the model, it was assumed that the flexure hinge was fabricated from S304 stainless steel with a Young's modulus of 193 GPa and a density of 7860 kg m^{-3}. The length, width and height of the seismic structure were specified as 15 mm, 15 mm and 34 mm, respectively, and the diameter of the flexure hinge was 14.25 mm. The FEA analysis indicated that the resonant frequency of the seismic structure was 93.13 Hz in both the X- and the Y-axis directions. Therefore, the resonant frequency characteristics of the seismic structure were in good agreement with the value of 100 Hz specified in the design stage.

The ANSYS FEM model was then employed to investigate the variation of the maximum stress and the maximum angular deflection of the seismic structure under different accelerations. Since according to the FE analysis, the two-dimensional seismic structure exhibits an identical resonant frequency response in the X- and Y-axis directions, the analysis considered variations of the stress and the angular deflection in the X-axis direction only. The ANSYS results indicated that the stress, σ, of the seismic structure under the different accelerations was given by σ (MPa) $=$ 30.47 (MPa g^{-1}) $\times$ acceleration (g), while the angular deflection, δ_θ, was given by δ_θ (μrad) $=$ 1297.5 (μrad g^{-1}) $\times$ acceleration (g).

The maximum permissible tensile stress of a flexure hinge is generally specified as 0.1–0.3 of its effective yield stress [16]. The effective yield stress of the S304 stainless steel material considered in the present study is 207 Mpa. Therefore, the maximum operational range of the current seismic structure is defined as the angular deflection of the flexure hinge corresponding to a maximum stress of 62.1 MPa (i.e. 30% of the effective yield stress). Accordingly, from the correlations identified in the ANSYS FEM analysis, the maximum acceleration measurement range in the X- and Y-axis directions was determined to be 2.04 g peak (i.e. 62.1/30.47), while the corresponding angular deflection of the seismic mass was specified as ± 2646.9 μrad (i.e. 2.04 $\times$ 1297.5).

Figure 10 presents a schematic illustration of the accelerometer constructed in accordance with the FEM design model. As shown, the seismic mass is suspended above the DVD pick-up head and both units are housed in a 2014-T6 aluminum casing. A reflective film is attached to the lower surface of the seismic mass and the position of the laser beam is adjusted until the reflected laser beam from the pick-up head is positioned at the centre of the four-quadrant photodiode, i.e. $X = Y = 0$. The accelerometer is then attached to the vibrating structure of interest. Vibrations of this structure cause a displacement of the seismic mass in the X- and Y-axis directions, and hence cause the focused light spot to move across the surface of the photodiode. As described previously, the shift of the focused light spot generates a corresponding change in the normalized voltage signals from the four quadrants of the photodiode, from which the acceleration applied to the base can be derived.

4. Experimental set-up and measurement results

4.1. Two-dimensional angle probe performance measurement

To investigate the measurement capabilities of the two-dimensional accelerometer, the experimental arrangement shown in figure 11 was established to calibrate the relationship between the angle of the seismic mass and the normalized output voltages in the X- and Y-axis directions, respectively. The pick-up head was fixed in position and a plane mirror was attached to a lever mechanism, which was attached in turn to a stationary surface via a notch-type flexure hinge of the same dimensions as that used in the accelerometer. The free end of the lever mechanism was driven by a precision piezoelectric ceramic linear motor (PCLM) micro-linear stage (Model Number HR-8, Nanomotion Ltd, Israel). The angular deflection of the lever mechanism was measured using an SIOS laser interferometer (Model Number SP 2000-TR, SIOS Co., Germany), and the corresponding variations in the normalized voltages in the X- and Y-axis directions, respectively, were detected using a data acquisition interface card (PCI-6036E, National Instruments, USA). The normalized voltages were computed using an analogue signal processing circuit according to equations (6) and (7). As with all diodes, the output power of the laser diode used in the

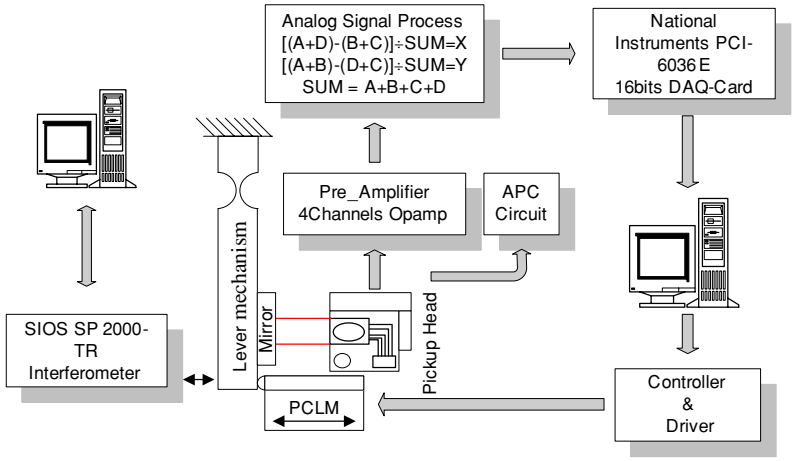

Figure 11. Experimental set-up for angle calibration.

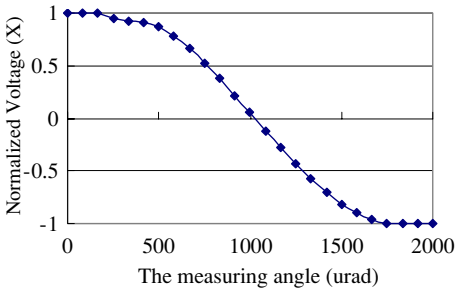

Figure 12. Variation of normalized voltage in the *X*-axis direction with angular displacement of lever mechanism.

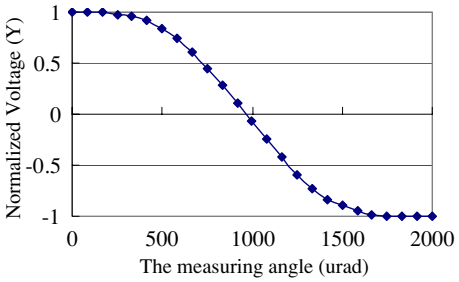

Figure 13. Variation of normalized voltage in the *Y*-axis direction with angular displacement of lever mechanism.

current experimental investigation is highly sensitive to the ambient temperature. Therefore, an APC circuit was used to maintain its stability during the calibration experiments.

Figures 12 and 13 plot the variation of the *X*-axis and *Y*-axis direction normalized voltages against the angular deflection of the lever mechanism. It is observed that the voltage curves are consistent with the theoretical results presented for the light intensity in figure 7. Figures 12 and 13 indicate that the two-dimensional angular displacement sensor has a linear range of approximately 500 μrad, extending from 650 μrad to 1150 μrad. It is noted that the stress induced in the flexure hinge by angular displacements in this linear range is well below the maximum allowable stress indicated by the ANSYS FEM analysis. Therefore, the linear range of

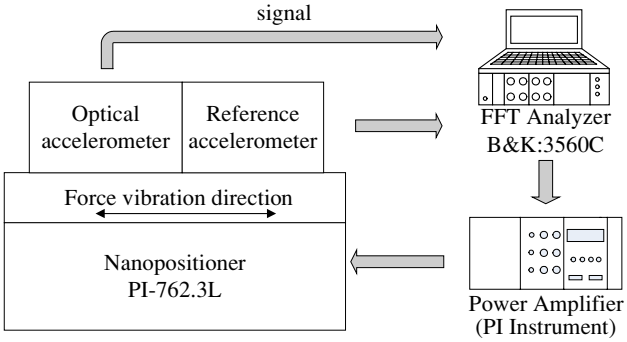

Figure 14. Experimental set-up for comparison calibration trials.

650 μrad to 1150 μrad represents an appropriate working range for the current two-dimensional accelerometer.

4.2. Accelerometer performance test

Once an accelerometer has been fabricated, its sensitivity and frequency response are essentially fixed. Therefore, any significant changes in these characteristics are likely the result of an unstable design, inappropriate use or external damage. In general, accelerometers are calibrated by recording their output under a particular excitation force and then comparing this output with that generated by a reference accelerometer subjected to the same excitation conditions. This comparison-type calibration method is straightforward, convenient and provides rapid results, and is therefore widely applied in many measurement and calibration laboratories. Accordingly, the present study employs the same approach to characterize the performance of the current optical accelerometer.

Figure 14 illustrates the experimental set-up established for the comparison calibration test. The current accelerometer was placed beside an ultra-low frequency reference accelerometer (Model Number 731A, Wilcoxon Research Inc., USA) on the stage of a three-axis nanopositioner (Model Number PI-762.3L, Physik Instrumente (PI) Co., Germany). During the calibration experiments, the nanopositioner was driven by excitation signals generated by an FFT analyser (Model Number 3560C, Bruel & Kjaer, Denmark) and

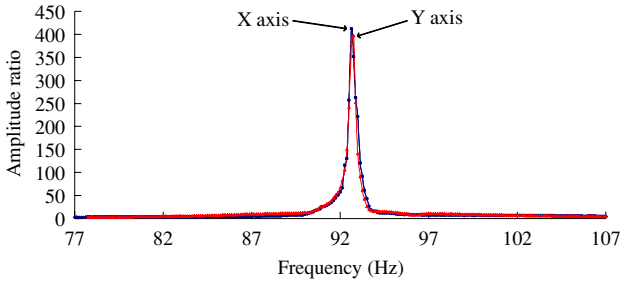

Figure 15. Frequency response in *X*-axis and *Y*-axis directions.

amplified by a power amplifier (Model Number E-501.00, Physik Instrumente (PI) Co., Germany). The output signals of the two accelerometers were acquired and analysed by the FFT analyser.

4.2.1. Resonant frequency measurement. The resonant frequency of the two-dimensional optical accelerometer was measured using the experimental set-up shown in figure 14. The FFT analyser was used to generate a swept sine waveform signal, which was amplified and then applied to the nanopositioner, causing it to vibrate in the *X*- or *Y*-axis direction. Due to the side-by-side arrangement of the two optical accelerometers, both instruments experienced the same oscillatory movement. The output signal from the reference accelerometer and the normalized voltage signals from the two-dimensional optical accelerometer were converted into corresponding displacement signals and passed to the FFT analyser, which then calculated the amplitude ratios of the two accelerometers every 0.125 Hz. Figure 15 presents the frequency response of the optical accelerometer in the *X*- and *Y*-axis directions, respectively. The results show that the resonant frequency of the accelerometer in the *X*-axis direction is 92.75 Hz, while that in the *Y*-axis direction is 92.875 Hz. Note that these values are 0.4% and 0.27%, respectively, lower than the resonant frequency of 93.13 Hz predicted from the FE analysis. It is also observed that the peak amplitude ratio of the resonant frequencies is 412.1. Substituting this amplitude ratio into equation (5), it is found that the damping ratio, ξ, of the current optical accelerometer is 0.0012 ($Q = 412.1$). In other words, the cantilever beam of the optical accelerometer has low damping.

4.2.2. Low-frequency acceleration response measurement. The experimental set-up shown in figure 14 was used to investigate the low-frequency acceleration response of the optical accelerometer. Using a forced vibration with a frequency well below the resonant frequency, the amplitude of the nanopositioner displacement was varied and the corresponding outputs of the reference accelerometer and optical accelerometer were recorded.

As stated previously, the optical accelerometer developed in the present study is designed to measure movements of the Earth's crust. Therefore, the experiments employed a sine waveform with a constant frequency of 10 Hz as the excitation signal and varied the amplitude of the nanopositioner displacement over the range 1–50 μm. Note that in the experiments, the excitation force was applied

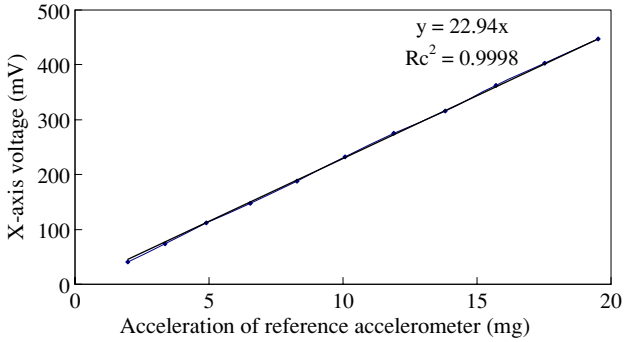

Figure 16. Low-frequency acceleration response in the *X*-axis direction for a driving frequency of 10 Hz.

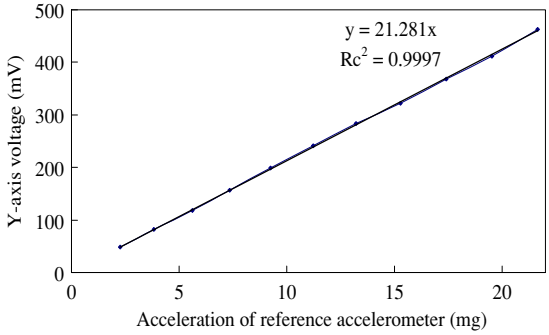

Figure 17. Low-frequency acceleration response in the *Y*-axis direction for a driving frequency of 10 Hz.

initially in the *X*-axis direction only, and then in the *Y*-axis direction only such that the responses of the accelerometer in the two directions could be individually identified. Figure 16 illustrates the variation of the normalized voltage of the proposed accelerometer in the *X*-direction with the applied acceleration (as determined by the reference accelerometer), while figure 17 shows the corresponding relationship between the normalized voltage in the *Y*-direction and the acceleration. From inspection, the sensitivities of the two-dimensional optical accelerometer in the *X*- and *Y*-axis directions are found to be 22.9 V/g and 21.3 V/g, respectively. The fitting accuracy can be evaluated by investigating the coefficient of correlation, R_c of the plotted data. R_c^2 is defined as the coefficient of determination and its value approaches unity as the fitting accuracy increases. Analysing the experimental data in figures 16 and 17, R_c^2 is found to have values of 0.9998 and 0.9997, respectively, indicating a high fitting accuracy in both cases. Furthermore, it is clear that the optical accelerometer has excellent linearity characteristics in both directions.

4.2.3. Frequency response measurement. Using the experimental set-up shown in figure 14, the FFT analyser was used to generate swept sine waveform signals with frequencies in the range of 0.5–23 Hz. The signals were amplified by the power amplifier and used to drive the nanopositioner, which was regulated such that it provided a constant displacement amplitude of 50 μm. The corresponding normalized voltage signals of the optical accelerometer in the *X*- and *Y*-axis directions were then converted into the corresponding accelerations using the sensitivity values obtained from

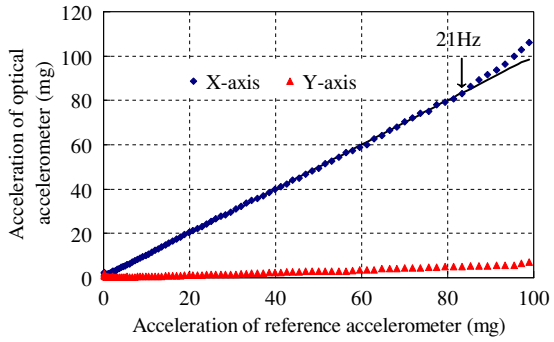

Figure 18. Low-frequency acceleration response in the *X*-axis direction for driving frequency in the range 0.5–23 Hz.

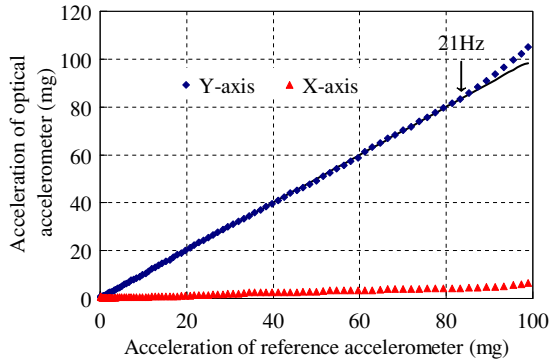

Figure 19. Low-frequency acceleration response in the *Y*-axis direction for driving frequency in the range 0.5–23 Hz.

figures 16 and 17, respectively. For comparison purposes, the FFT analyser also recorded the acceleration of the reference accelerometer every 0.25 Hz. Figure 18 plots the variation of the acceleration of the optical accelerometer in the *X*-axis direction against the acceleration values obtained using the reference accelerometer when the excitation force was applied in the *X*-axis direction. Similarly, figure 19 shows the relationship between the acceleration of the optical accelerometer in the *Y*-axis direction and the acceleration of the reference accelerometer when the driving force was applied in the *Y*-axis direction. It can be seen that the acceleration results obtained using the optical accelerometer are in good agreement with those of the reference accelerometer at operating frequencies below 21 Hz. Furthermore, it is observed that a coupling of approximately 6% exists between the acceleration in the driven axis direction and that induced in the non-driven axis direction.

4.2.4. Noise equivalent acceleration (NEA) measurement. To measure the NEA of the optical accelerometer, the noise of the normalized voltages in the *X*- and *Y*-axis directions, respectively, was recorded by the FFT analyser when the nanopositioner was turned off, i.e. the optical accelerometer was stationary. The noise signals were then converted into corresponding NEA spectral densities by applying the sensitivity values calculated from figures 16 and 17, respectively. Figures 20 and 21 plot the NEA spectral densities in the *X*- and *Y*-axis directions, respectively, against the frequency. It can be seen that the electronic circuitry of

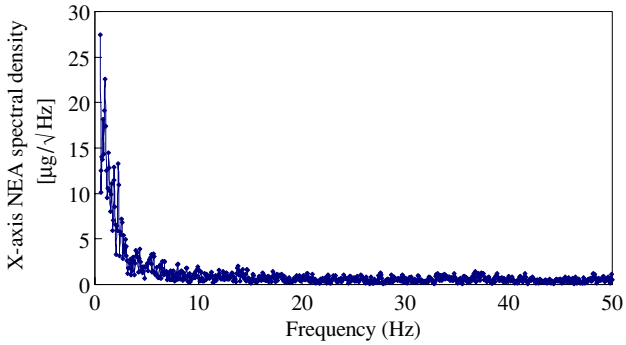

Figure 20. Variation of NEA spectral density in the *X*-axis direction over the frequency range 0.5–50 Hz.

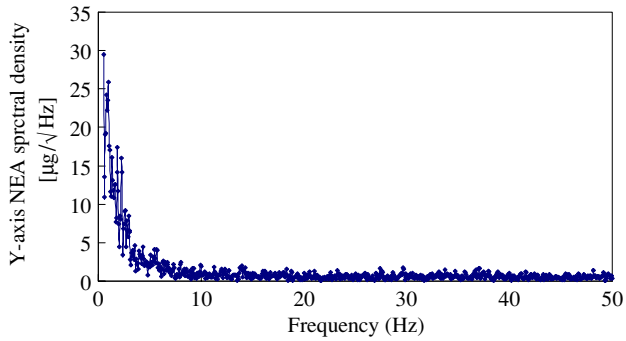

Figure 21. Variation of NEA spectral density in the *Y*-axis direction over the frequency range 0.5–50 Hz.

the optical accelerometer generates an electrical noise of less than 30 μg Hz$^{-1/2}$ over the frequency range 0.5–50 Hz.

5. Conclusions

This study has presented a low-cost, highly sensitive two-dimensional optical accelerometer comprising a two-dimensional seismic structure suspended using a notch-type flexure hinge and a modified commercial DVD pick-up head. The experimental results have shown that the resonant frequencies of the accelerometer in the *X*- and *Y*-axis directions are 92.75 Hz and 92.87 Hz, respectively. Furthermore, the sensitivities of the accelerometer in the *X*- and *Y*-axis directions are 22.9 V/g and 21.3 V/g, respectively. Finally, the accelerometer has a NEA of less than 30 μg Hz$^{-1/2}$ over the frequency range 0.5–50 Hz. The performance of the accelerometer compares favourably with that of commercially available ultra-low frequency high-sensitivity accelerometers.

The accelerometer developed in this study is designed to measure the acceleration of the Earth's crust and that of other low frequency vibration generators, such as subways, buses, tides, the wind and so on. Therefore, the useful frequency range is specifically restricted to the range 0.5–21 Hz, i.e. approximately 20% of the resonant frequency of the seismic structure. However, the useful frequency range can be increased by changing the dimensions of the seismic structure to increase its structural stiffness or to reduce its seismic mass. The system can then be applied to the acceleration measurement of a broader range of vibrational

fields, such as machine tools, robotics, navigation systems, motor vehicles, missile control systems and so forth.

Acknowledgments

The present authors gratefully acknowledge the support provided to this project by the National Science Council, Taiwan, ROC under contract nos. NSC94-2212-E-218-010 and NSC94-2212-E-002-028.

References

[1] Serridge M and Licht T R 1987 *Piezoelectric Accelerometers and Vibration Preamplifiers* (Denmark: Bruel and Kjaer)
[2] Doeblin E O 1990 *Measurement System: Application and Design* 4th edn (New York: McGraw-Hill)
[3] Meydan T 1997 Recent trends in linear and angular accelerometers *Sensors Actuators* A **59** 43–50
[4] Fang X and Cao M 2003 Theoretical analysis of 2D acceleration laser sensor and several design parameters *Opt. Laser Technol.* **35** 345–8
[5] Fang X and Cao M 2002 Theoretical analysis of 2D laser angle sensor and several design parameters *Opt. Laser Technol.* **34** 225–9
[6] Dinev P D 1995 A two-dimensional fibre-optical vibration sensor *Meas. Sci. Technol.* **6** 1395–8
[7] Dinev P D and Dinev T S 1998 Optical accelerometer *US Patent* 5,837,998
[8] Armstrong T R and Fitzgerald M P 1992 An autocollimator based on the laser head of a compact disc player *Meas. Sci. Technol.* **3** 1072–6
[9] Quercioli F, Mannoni A and Tiribilli B 1997 Correlation optical velocimetry with a compact disk pickup *Appl. Opt.* **36** 6372–5
[10] Zhang J H and Cai L L 1997 An autofocusing measurement system with a piezoelectric translator *IEEE/ASME Trans. Mechatron.* **2** 213–6
[11] Fan K C, Chu C L and Mou J I 2001 Development of a low-cost autofocusing probe for profile measurement *Meas. Sci. Technol.* **12** 2137–46
[12] Fan K C, Chu C L, Liao J L and Mou J I 2003 Development of a high precision straightness measuring system with DVD pick-up head *Meas. Sci. Technol.* **14** 47–54
[13] Benschop J and Rosmalen G V 1991 Confocal compact scanning optical microscope based on compact disc technology *Appl. Opt.* **30** 1179–84
[14] Chu C L and Lin C H 2005 Development of an optical accelerometer with a DVD pick-up head *Meas. Sci. Technol.* **16** 2498–502
[15] Sony semiconductor product list 1999, Sony Co., Photo Device KHM-210AAA 1999
[16] Smith S T and Chetwynd D G 1992 *Foundations of Ultraprecision Mechanism Design* (London: Gordon and Breach) pp 95–104